

**Atomic-scale modeling of the dissolution of oxidized platinum nanoparticles in an explicit water environment**

Journal:	<i>Journal of Materials Chemistry A</i>
Manuscript ID	TA-ART-11-2022-009152.R2
Article Type:	Paper
Date Submitted by the Author:	23-Feb-2023
Complete List of Authors:	Slapikas, Robert; The Pennsylvania State University, Materials Science and Engineering Dabo, Ismaila; The Pennsylvania State University, Materials Science and Engineering Sinnott, Susan B. ; The Pennsylvania State University, Materials Science and Engineering

*Journal of Materials Chemistry A***Atomic-scale modeling of the dissolution of oxidized platinum nanoparticles in an explicit water environment**Robert E. Slapikas^{1,2}, Ismaila Dabo^{2,3,4}, Susan B. Sinnott^{2,3,4,5,*}

1. Applied Research Laboratory, The Pennsylvania State University, University Park, PA 16802, United States
2. Materials Science and Engineering Department, The Pennsylvania State University, University Park, PA 16802, United States
3. Materials Research Institute, The Pennsylvania State University, University Park, PA 16802, United States
4. Institutes of Energy and the Environment, The Pennsylvania State University, University Park, PA 16802, United States
5. Department of Chemistry, The Pennsylvania State University, University Park, PA 16802, United States

***Corresponding Author:**Email: sinnott@matse.psu.edu**Abstract**

Pt nanoparticles (NPs) are currently being investigated for use in fuel cells; however, Pt NP oxidation as a function of size, morphology, and temperature is not well understood or currently quantified. In this study, the stability and dissolution of oxidized platinum NPs is examined via classical molecular dynamics in an explicit water environment. The NPs considered range in size from 1.35 to 2.92 nm in diameter and included five different monolayer (ML) coverages of O*. The simulations were performed at 300, 450, and 600 K with the many-body, reactive third-generation charge-optimized many-body or COMB3 potentials and examine the kinetics of NP dissolution in water. The Pt-O layer, which reduces the kinetic activity for Pt atom dissolution, is projected to make dissolution more favorable for O* MLs smaller than 0.5. The simulations further indicate that the Pt NPs' kinetic rates of dissolution are slowed by an increase in the number of adsorbed species caused by the dissociation of water molecules at the reconstructed facets of the Pt NPs. These findings quantify the effect of oxygen and temperature on the stability and dissolution of oxidized platinum NP in an explicit water environment similar to the conditions in fuel cells and electrocatalysis.

Introduction

In electrochemistry solid-liquid, electrode-electrolyte interface regulates electrochemical processes that are essential for energy storage and production, such as those found in fuel cell technologies, electrochemical sensors, and medical equipment.¹⁻³ Currently, metallic nanoparticles (NPs), specifically those containing Pt, have been found to improve the sluggish catalytic activity of oxygen reduction reactions (ORR).¹⁻⁵ This is because the small size of the NPs maximizes the surface area, and Pt's intrinsic electronic structure makes it an effective catalyst.^{1,5} But while Pt is an excellent electrocatalyst for polymer electrolyte membrane fuel cells (PEFCs), the high cost of Pt remains a deterrent for commercialization.^{1,5,6} Therefore, a fundamental understanding of the reactions occurring at the electrode-electrolyte interfaces is important to ensure their most efficient utilization.⁷

Currently it is accepted that the degradation of Pt NPs occurs first through oxidation, and then through the dissolution of Pt atoms in PEFCs.²⁻⁴ Experimentally, these electrochemical processes have been investigated using cyclic voltammetry, X-ray diffraction, X-ray absorption spectroscopy, scanning electron microscopy, transmission electron microscopy, scanning tunneling microscopy, and high-resolution inductively coupled plasma mass spectrometry.^{1,6} It has been determined through these investigations that the oxidation and dissolution of atoms from electrode surfaces during ORR affect the materials' durability and catalytic performance.^{8,9} This is related to the electrochemical active surface area (ECSA), where both Pt dissolution and ECSA both drop down precipitously as NPs increase in size.¹⁰⁻¹² Through oxophilicity, the NPs are rendered less susceptible to dissolution by the formation of oxide layers. Research of these materials and their surfaces at the atomic level further explains the structure-property relationships that govern ORR and electrode degradation.¹³

These experimental studies can be complemented with computational models to enhance the understanding of the kinetic reactions and can be used to predict the response of oxidation and electrode dissolution in electrochemical environments. Over the past decade several computational techniques have been used to describe the mechanisms that control ORR.^{4,5,14,15} For instance, density functional theory (DFT) and quantum statistics have been used to describe electrochemical reactions at steady state. With DFT, Pt-O surface interactions have been extensively studied to determine how different Pt surfaces respond to electrochemical environments.^{4,16-19} DFT is a powerful tool for predicting ORR events as it is able to describe the electron transfer and charge accumulation at the surface, along with molecular polarization at the solid-liquid interface.¹⁶ Often, these calculations employ a small number of atoms and use only a few adsorbed species due to the high computational cost.^{13,14,20,21}

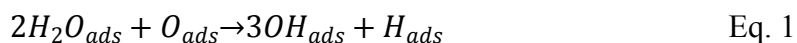
Atomic cluster expansion is another technique used to study the local electrochemical environments mainly studying alloy systems and surface adsorption,^{22,23} where the analysis of these modes are equilibrium structures are trained from DFT data.^{22,24} Although these models have shown merit and are even programed into large scale codes, for them to correctly model electrochemical interactions the models still need well defined descriptors and still have to deal with the use of implicit solvents.²²⁻²⁵ Therefore, to increase the size of these calculations, catalytic surfaces can be run in an implicit electrolyte environment; however, these calculations lack the physics and chemistry to describe the mechanisms associated with atomic dissolution through interactions with explicit water molecules.^{13,20,26} With these models, it has been understood that large-scale simulations that incorporate charge transfer between atoms are required to adequately model electrochemical interactions.^{14,20,27} Such interactions include creating and stabilizing the surface structures on metal electrodes, or metal-ion solution interactions. However, a realistic

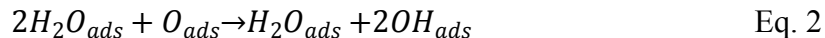
physical model of polarization and charge transfer between atoms is either extremely difficult or computationally impossible to implement in large scale simulations. Currently, classical molecular dynamics (MD) simulations may accomplish this by using reactive potentials that incorporate the electronegativity equilibration charge system (QEq) method.^{28,29} This technique can simulate the electrode surfaces and NP architectures that will affect ORR, as well as the dissolution of the NPs using traditional computational models. These simulations remain minuscule compared to the length scales needed to accurately model real-world conditions.⁷

Previously, work has been conducted using classical MD simulations and the electronic charge-optimized many body (e-COMB) reactive potential was applied to examine a Cu electrode with a water electrolyte comprising of OH⁻ and H⁺ ions.³⁰ Charge transfer between the electrode and electrolyte atoms was simulated utilizing two distinct QEq schemes, one for the electrolyte and one for the electrode.³⁰ This configuration was chosen due to the constraints of the charge transfer scheme and the need for a constant applied electronegativity offset.³⁰ However, it has been determined in previous work that implementing separate QEq schemes for the electrode-electrolyte interface makes it impossible to replicate important electrochemical phenomena, such as a sacrificial anode, due to incorrect dynamics and inaccurate charge transfer behavior.³¹ This was also further studied in the oxidation of Pt NPs, where their stability was studied for five different monolayer (ML) coverages of oxygen adsorbates (O*) for different morphologies and sizes comparable to experimental results.³² These simulations are typically challenging to produce due to the reactions needed and the size of these simulations, where most applications for Pt NP have a size range of 1-5 (nm) and this causes the number of atoms in each simulation to run from 85-5000 atoms. However, with the optimization of the COMB3 potential simulations with over 45,000 atoms were possible where the Pt NPs had a diameter of 11.3 nm.^{31,32} Despite efforts to improve

the description of this interface, numerous obstacles still remain to modelling it at the atomic and electronic scales, including charge accumulation on electrode surfaces, correct charge transport, and simulation size limitations. As a result, a single QEq scheme is employed to characterize both the electrode and the electrolyte for accurate replication of electrochemical events.^{31,32}

The focus of this work is to investigate the surface reactivity of oxidized Pt NPs and define the kinetics of NP dissolution in an explicit water environment, while analyzing the effects of different oxygen-binding sites and the influence of NP size on these reactions. This is to address the durability of Pt NPs commonly used in PEFCs as catalyst materials. The MD simulations use explicit interactions of the water electrolyte with Pt NPs and the electrodes so to create a foundational insight on charge transfer at the electrode-electrolyte interface, and to understand their influence on Pt atom dissolution. The simulation results are compared to the results of DFT calculations of Pt NPs and Pt surface in implicit water environments. The results of these calculations indicate that the (100) facet of Pt NPs is especially prone to dissolution near edge and corner site, and that water molecules readily dissociate at higher index facets.^{33–35} With this, it is believed that the dissociation of water molecules occurs at the facets of the NPs. Dissociation is also thought to occur at higher rates for higher ML coverages, due to the high ratio of oxidized Pt surfaces and adsorbed oxygen atoms available for reactions with adsorbed water molecules.^{34,36} This higher dissociation rate has also been predicted in DFT data for high-index facets. Equation 1 shows what is believed to be the dissociation reaction, after which the Pt NP will contain three OH⁻ adsorbates and one H⁺ ion for every two water molecules and one adsorbed O atom.³⁷ However, Equation 2 was previously determined through first-principles calculations to be the energetically favorable reaction.³⁷





Computational Details

Classical MD simulations were carried out using the open-source code Large-scale Atomic/Molecular Massively Parallel Simulator (LAMMPS) and the previously parameterized third-generation charge-optimized many body (COMB3) reactive interatomic potential for Pt-O-H.^{38,39} The ability to accurately characterize metal H₂O interactions and hydrogen bonds concurrently is required for this endeavor and it was established that the potential correctly anticipated the nanoscale architectures of water on Pt surfaces and even the buckled bi-layer of water on the Pt (111) surfaces. This is made possible by using the variable QEq scheme, which is implemented in LAMMPS for COMB3.⁴⁰ Enabling accurate measurements of electrostatic environments, the COMB3 potential has demonstrated in MD investigations the effects that adsorbed species on Cu (111) surfaces have on the wetting of explicit water nanodroplets. The functional form of COMB3 is described by the total potential energy (U_{tot}) which is the summation of atoms' ionization energies and electron affinities (U_{self}), the reactive short-range interactions (U_{short}), the Coulombic interactions (U_{Coul}), the angular correction term (U_{corr}), the atomic polarizability (U_{polar}), and the van der Waals energy (U_{vdW}), where the positions and charges of individual atoms are denoted by r^N and q^N respectively, as outlined in Equation 3.⁴⁰

$$U_{tot}(r^N, q^N) = U_{self}(q^N) + U_{short}(r^N, q^N) + U_{Coul}(r^N, q^N) + U_{corr}(r^N) + U_{polar}(r^N, q^N) + U_{vdW}(r^N) \quad \text{Eq. 3}$$

In these simulations, we considered oxidized Pt NPs with five different O* monolayer coverages (ML) (0, 0.25, 0.5, 0.75, 1.0) from previous work.³² In an effort to reduce the amount of computational resources needed to investigate all possible adsorption sites for this initial fundamental analysis, only the preferred adsorption site for oxygen atoms on the Pt (111) facets is used for the O* initial positions.^{19,41} This adsorption site on the Pt (111) facets is face-centered

cubic (FCC) hollow site. The Pt (111) facets are used for the adsorption surfaces in this study, because experimentally it is seen the equilibrium shapes of Pt NPs is primarily restricted due to the low surface energy of this facet.^{42,43} The modeled oxygen monolayer coverages correspond to those on the NPs after the application of an external voltage in, e.g., a fuel cell and a strong correlation has been shown that increasing the applied potential on the fuel cell increases the oxide coverage on the Pt NPs.^{44–46} An increase in the temperature of the cell has a much smaller impact on the oxide film growth rate.^{45,46} Even though we are not applying an external potential in these simulations, the coverages modeled are comparable for the entire range of possible oxygen coverage on NPs under operational fuel-cell conditions.¹⁴

Once each oxidized Pt NP reached thermodynamic equilibrium, it was immersed in explicit water, and the new system was allowed to evolve in order to observe the possible dissolution of the Pt NPs, where in all the simulations the polar-off flag is used. The density of the water in the simulation box is given by Equation 4. In the initial simulation builds the density of the water within 3 Å from the Pt NP surface is taken to be 1.09 g/cm³ and the density of water farther than 3 Å from the Pt NP surface is taken to be 1.00 g/cm³. In this equation, Pt NP_{SA} is the surface area of the NP, Pt NP_{Vol} is the volume of the NP, and R_{pt} is the radius of the Pt NP. The initial builds are first created by adding the reconstructed Pt NP to the desired simulation cell then water molecules are added around the NP in the simulation cell with the packmol software package with varying densities as previously stated.⁴⁷

$$\text{water density in simulation} = \frac{((Pt\ NP_{SA} * 3\text{\AA}) * 1.09\frac{g}{cm^3}) + ((Pt\ NP_{Vol} - [Pt\ NP_{SA} * 3\text{\AA}]) * 1.00\frac{g}{cm^3})}{Initial\ Vacuum\ Volume} \text{ Eq. 4}$$

In order to achieve a preliminary understanding of the kinetic effects of water on the Pt NPs, simulations are performed at 300, 450, and 600 K. Although these temperature ranges exceed

the operating temperatures of most PEFCs, using higher temperatures in the MD simulations speeds up the kinetic reactions and reduces the amount of CPU wall time needed.^{10,14,48} The selected Pt NPs used in this work range in size from 1.35 nm to 2.92 nm and are depicted in Figure 1 with 1 ML of O*. The NPs used are of two different morphologies the Pt (111) facet NPs (Wulff construction) which are labeled as just the number of atoms in the NP and the Pt (110) facet NPs where a prime is appended to the number of Pt atoms in the NP. These NPs were selected since the size range is a little more than half of the commonly used application sizes of Pt NPs (1-5 nm) and due to the large amount of CPU wall time needed to run the 240 simulations for the selected NPs in this work.^{14,49} Two Langevin thermostats were implemented, one to control the water temperature and one to control the temperature of the oxidized NPs.⁵⁰⁻⁵²

Using previously optimized input parameters of a timestep of 0.4 fs, charge equilibration every 50 timesteps, and a 0.1 ps relaxation time for the Langevin thermostats, reduced the necessary amount of CPU wall time of these simulations by 90%.³¹ In these simulations, Pt atoms are considered dissolved once the Pt atoms have a Pt-Pt nearest neighbor distance greater than 6 Å, which was determined from the vibrational frequency and the radial distribution function of the Pt-Pt interactions for a Pt atom on the surface of the Pt NPs.

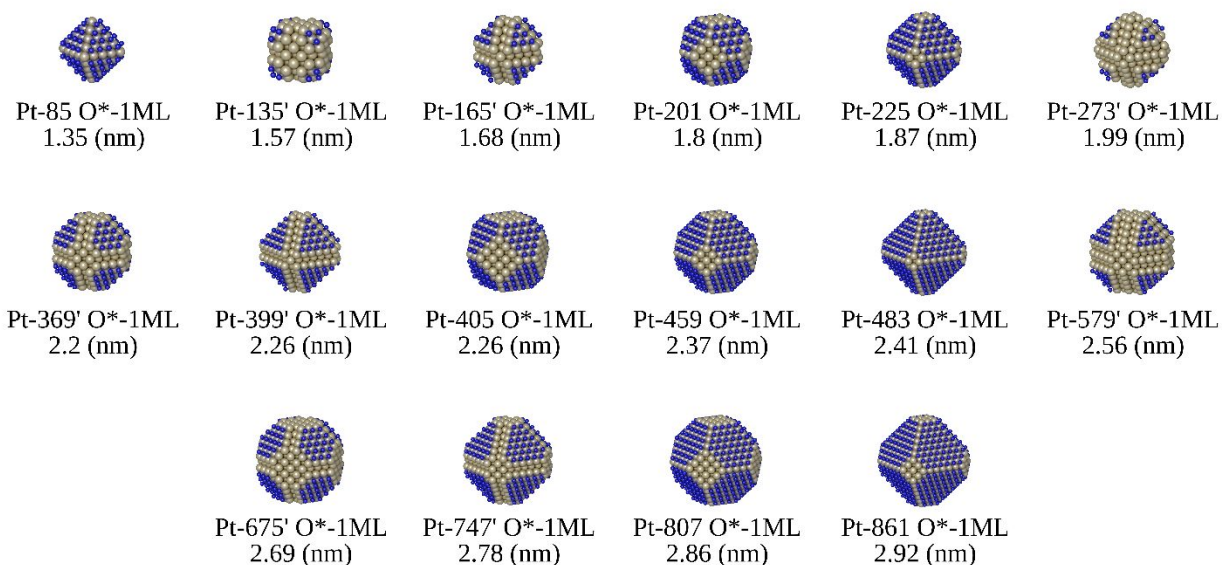


Figure 1- Structural models of platinum nanoparticles with a 1 ML oxygen adsorbates (O*) coverage used in explicit water MD simulations. The number of Pt atoms in each NP are labeled in each image of increasing size up to 861 Pt atoms. In this image the Pt atoms are colored grey and oxygen adsorbates are colored blue. When referring to Pt (110) facet NPs, a prime is appended to the number of Pt atoms in the NP, however no prime is appended to the label when referring to Pt (111) facet NPs (Wulff construction).

Results

The dissolution of Pt atoms from the oxidized NPs in water is predicted in the MD simulations, as illustrated in Figure 2. At 600 K, the simulations reveal that Pt dissolution starts at around 0.40 ns, with the Pt (100) facet atoms being the first to dissolve. As simulation time increases, the number of dissolved Pt atoms increases, as shown in Figure 3. Displayed in Table 1 are the average charges of the different types of Pt atoms in a MD-simulated oxidized Pt NP in an explicit water environment. In the COMB3 potential, dissolved Pt atoms with a positive charge greater than $+1 e$ indicate they have a maximum positive charge for the MD simulations. It should be noted that while the simulations indicate that the Pt atoms are moving from the NP to solution, we are unable to predict the oxidation state of the dissolved Pt atoms. This is a result of the use of the empirical potentials that do not describe electrons explicitly.

The atomic charge values of the surface, subsurface, and bulk Pt atoms are $+0.426 e$, $-0.226 e$, and $+0.02 e$, respectively. These values indicate that the bulk Pt in the NP is essentially neutrally charged, while the surface Pt atoms are positively charged at a value that is roughly half of a dissolved Pt atom. The subsurface Pt atoms are negatively charged which is a result of the physics implemented into QEq charge equilibration scheme and the COMB3 potential, which constantly drives the MD system to an overall simulation charge neutral state for the system conditions, this result in the Pt NPs having a shell charge is also predicted to occur under experimental conditions.

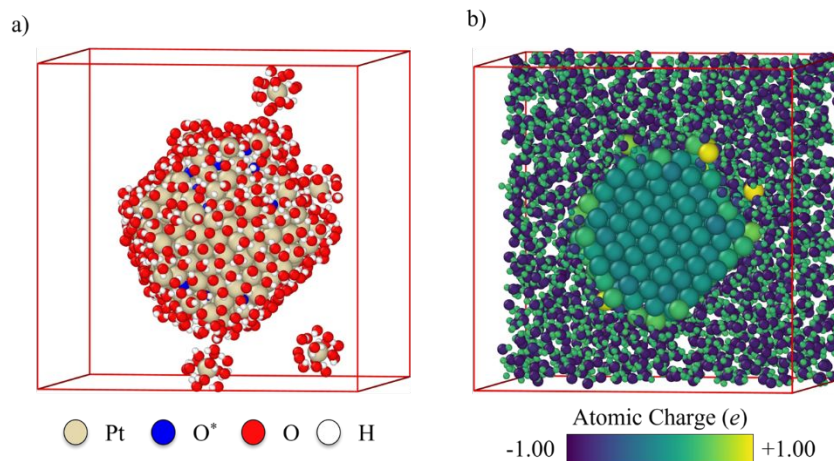


Figure 2 – a) Predicted dissolution of Pt and water molecules through a singular charge equilibration scheme. In the image only the water atoms near the Pt atoms are shown for visualization. B) Charge per atom of adsorbed water on the Pt-O* nanoparticles. The image is a slice of only half of the simulation cell for ease of visualization.

Pt – 807 – 0.25 ML – 600 K

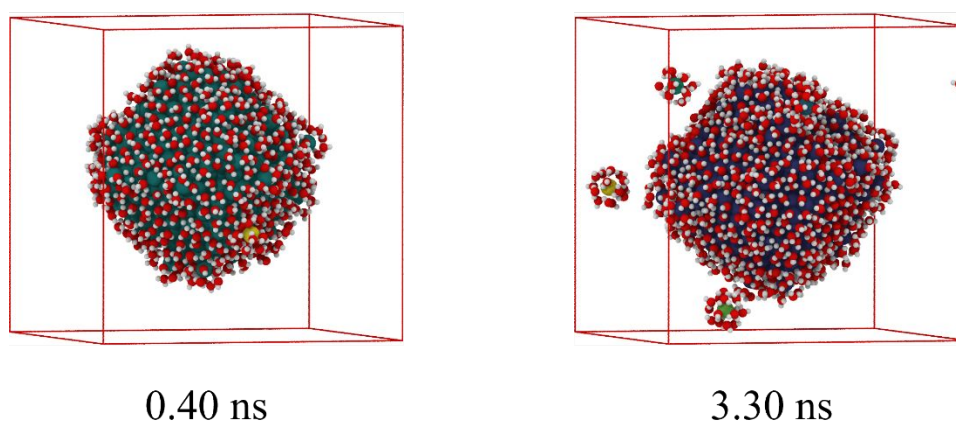
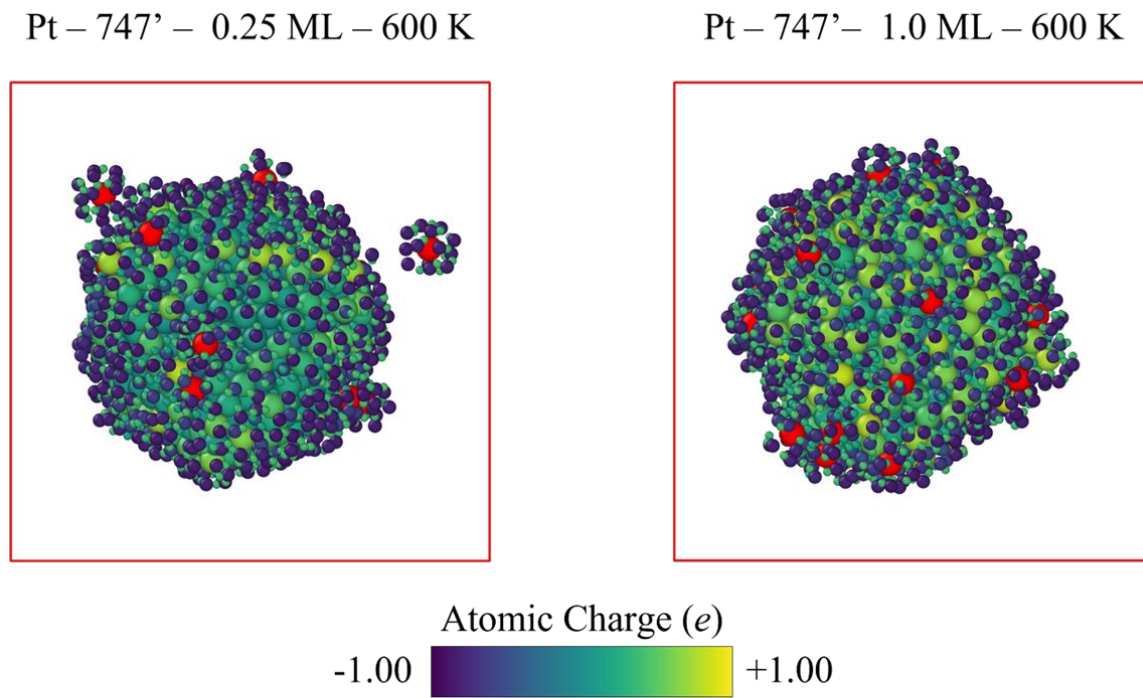


Figure 3 – Pt NP dissolution times and average charges of atoms in an 807 Pt NP with a 0.25 ML coverage at 600 K. Where the dissolution of the first Pt atom is predicted at 0.40 (ns), then then the simulated times of dissolution of the next four atoms are 0.98 (ns), 1.20 (ns), 1.46 (ns), and 2.33 (ns). In the image the water molecule atoms are colored red for oxygen and white for hydrogen. The Pt atoms are also colored by the bulk NP (dark green) and the individual dissolved Pt atoms. At 0.40 (ns) the first dissolved Pt atom is colored yellow, and at 3.30 (ns) it is possible to visually see three of the dissolved Pt atoms.

Table 1: Atomic average charge of Pt atoms in explicit water with Pt dissolution from the MD simulations

Pt atom type	Charge on atoms
Dissolved Pt atom	+1.036 <i>e</i>
Surface Pt atom	+0.426 <i>e</i>
Subsurface Pt atom	-0.226 <i>e</i> (max)
Bulk Pt atom	+0.02 <i>e</i>

Although it is predicted the atoms from the Pt (100) facet are the first to have dissolution, in these simulations, the charge quantity necessary to produce dissolution does not seem to have a threshold. Figure 4 displays an illustration of atoms colored according to their atomic charge, with red highlighting the atoms with charges more than 0.85 *e* which is roughly double the average charge of the Pt surface atoms. This image shows that certain atoms of the Pt 747 NP with an O* 0.25 ML have already dissolved from the NP having a charge greater than 0.85 *e*, while some have not dissolved. However, for the Pt 747 NP with an O* 1.0 ML, no atoms have undergone dissolution after 3.3 ns, despite some of the atoms having charge values greater than 0.85 *e*. It is also noted that although the average charge of a dissolved Pt atom is above +1 *e* there are some dissolved Pt atoms seen with charges as low as +0.75 *e*.



- Red atoms have a charge above $+0.85 e$
- Water atoms not near Pt atoms are omitted for visualization

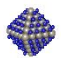
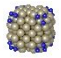




Figure 4 – Dissolution of Pt and water molecules is predicted not as a result of unique charge threshold. In the image on the left some atoms with a charge greater than $+0.85 e$ have dissolution at a O^* ML coverage of 0.25 while none of the atoms with a charge greater than $+0.85 e$ have dissolution at a O^* ML coverage of 1.0.

The prediction for Pt NP dissolution is further strengthened by examining the number of O^* as a percentage of the number of Pt surface atoms for each NP. It is possible to see all of the NP sizes simulated in this work and at which temperatures and O^* ML coverages that predicted Pt atom dissolution occurs, in Table 2. In this table the first column provides an image of each Pt NP and its corresponding size, then the second column shows the simulation temperature, and the third column lists the O^* ML coverages that Pt dissolution is predicted for the NP in column one. In these simulations, the dissolution of Pt atoms is only observed at two simulation temperatures: 450 K and 600 K. Figures 5-7, depict which NPs are predicted to undergo dissolution on the

timescales of these classical MD simulations and those that are not predicted to do so. As indicated in Figure 5, at 300 K, there is no observable dissolution in the MD simulations. While, it is expected that the dissolution of Pt atoms will occur at this temperature, the rates of these kinetic phenomena are likely to occur on timeframes that are still inaccessible to classical MD simulations.

It is predicted that the dissolution of Pt occurs more rapidly with an adsorbed oxygen ML coverage smaller than 0.5, while dissolution at 1.0 ML is almost non-existent, and only occurs at a temperature of 600 K for the Pt-135, Pt-273 and Pt-369 NPs. However, with a simulation temperature of 450 K, it is seen that neither end of the ML coverage spectrum is truly favorable for dissolution, as illustrated in Figure 6. However, in Figure 7, it is possible to see that at a simulation temperature of 600 K, dissolution mainly occurs when the ratio of O* is less than 40-50% of the number of Pt NP surface atoms, where it is predicted that the dissolution of Pt atoms is suppressed at the higher ratios due to the formation of a passive Pt oxide film as the O* ML coverage increases, and the oxidation and reconstruction of the initial NP increases. The only NPs that dissolution was predicted above this threshold of 50% are the Pt-405, the Pt-483, and the Pt-807 which all have a O* ML of 0.75. It is also noted that there are 5 NPs where the simulations observed Pt dissolution at a temperature of 450 K but did not observe dissolution at 600 K. Where 4 of these NPs (Pt-165', Pt-201, Pt-459', and Pt-807) have a O* ML coverage of 0.5, and the Pt-399' NP had a 0.75 ML coverage. It is also noted that for the NPs at 450 K where dissolution is predicted do not have the same initial morphology, with three of the NPs possessing the Pt (110) facets and two of the NPs possessing Pt (111) facets (Wulff constructions).

Table 2. – Pt NP's with predicted dissolution for specific O* ML coverages in an explicit water environment

NP Size	Simulation Temperature	Oxygen Adsorbate Monolayer Coverage where Pt Dissolution Occurs
 Pt-85 O*-1ML 1.35 (nm)	300 K	N/A
	450 K	0.0, 0.25
	650 K	0.0, 0.25
 Pt-135 O*-1ML 1.57 (nm)	300 K	N/A
	450 K	0.5, 0.75
	650 K	0.0, 0.25, 0.5, 0.75, 1.0
 Pt-165 O*-1ML 1.68 (nm)	300 K	N/A
	450 K	0.5
	650 K	0.0, 0.25, 0.75
 Pt-201 O*-1ML 1.8 (nm)	300 K	N/A
	450 K	0.25, 0.5
	650 K	0.25
 Pt-225 O*-1ML 1.87 (nm)	300 K	N/A
	450 K	0.25
	650 K	0.0, 0.25, 0.5
 Pt-273 O*-1ML 1.99 (nm)	300 K	N/A
	450 K	0.5
	650 K	0.0, 0.25, 0.5, 0.75, 1.0
 Pt-369 O*-1ML 2.2 (nm)	300 K	N/A
	450 K	N/A
	650 K	0.0, 0.25, 0.5, 0.75, 1.0
 Pt-399 O*-1ML 2.26 (nm)	300 K	N/A
	450 K	0.25, 0.75
	650 K	0.0, 0.25, 0.5
	300 K	N/A
	450 K	0.5

 Pt-405 O*-1ML 2.26 (nm)	650 K	0.25, 0.5, 0.75
 Pt-459 O*-1ML 2.37 (nm)	300 K	N/A
	450 K	0.25, 0.5
	650 K	0.0, 0.25
 Pt-483 O*-1ML 2.41 (nm)	300 K	N/A
	450 K	N/A
	650 K	0.0, 0.25, 0.5
 Pt-579 O*-1ML 2.56 (nm)	300 K	N/A
	450 K	N/A
	650 K	0.0, 0.25, 0.5, 0.75
 Pt-675 O*-1ML 2.69 (nm)	300 K	N/A
	450 K	N/A
	650 K	0.0, 0.25, 0.5, 0.75
 Pt-747 O*-1ML 2.78 (nm)	300 K	N/A
	450 K	0.5
	650 K	0.25, 0.5, 0.75
 Pt-807 O*-1ML 2.86 (nm)	300 K	N/A
	450 K	0.5
	650 K	0.0, 0.25, 0.75
 Pt-861 O*-1ML 2.92 (nm)	300 K	N/A
	450 K	0.25
	650 K	0.0, 0.25

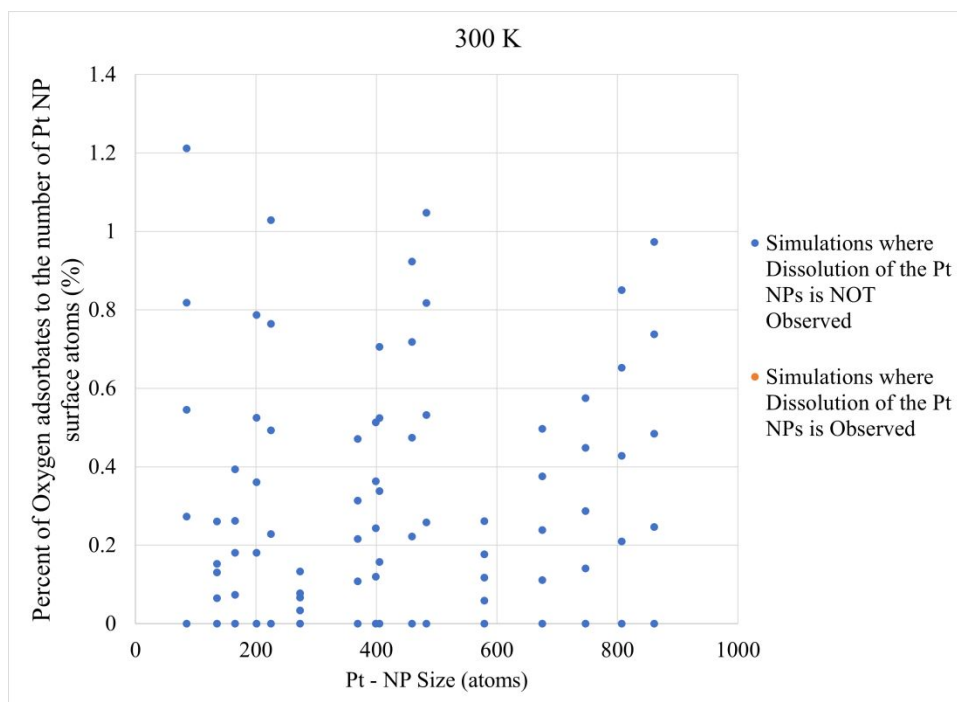


Figure 5 – Illustration of which Pt NPs undergo dissolution at 300 K, showing the relationship to Pt-NP size (number of atoms), and to the number of oxygen adsorbates as a percentage of the number of Pt NP surface atoms (%). In the simulations run at 300 K, dissolution of the Pt NPs was not observed in any of the MD simulations.

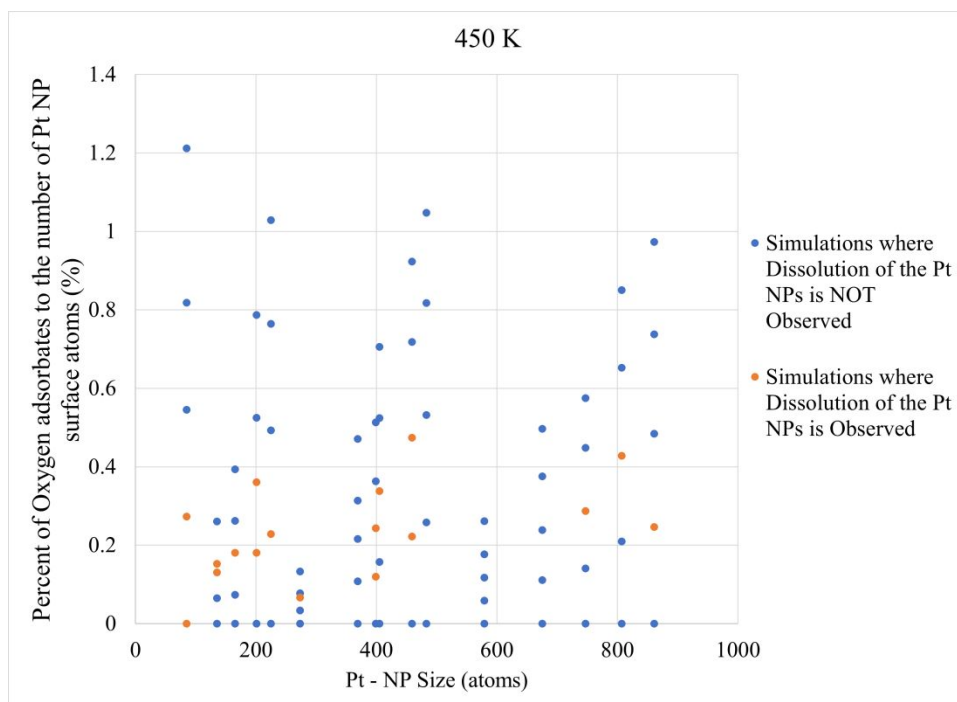


Figure 6 - Illustration of which of the Pt NPs have dissolution at 450 K, showing the relationship to Pt-NP size (number of atoms), and to the number of oxygen adsorbates as a percentage of the number of Pt NP surface atoms (%).

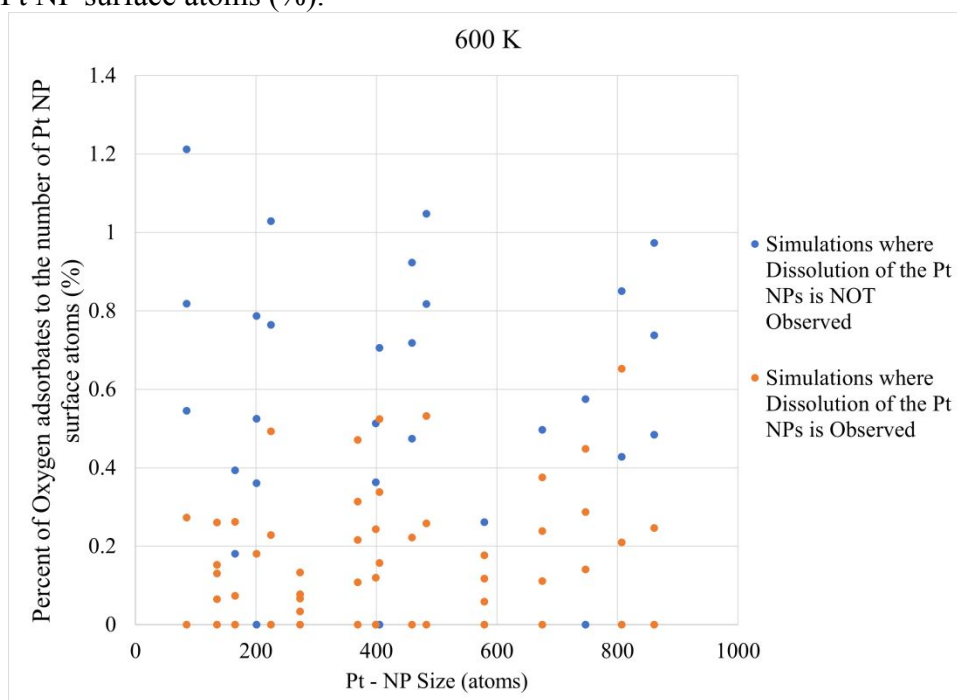


Figure 7 - Illustration of which of the Pt NPs have dissolution at 600 K, showing the relationship to Pt-NP size (number of atoms), and to the number of oxygen adsorbates as a percentage of the number of Pt NP surface atoms (%).

Discussion

In this paper, a reproducible model of classical MD simulations predicting Pt dissolution is developed utilizing a reactive interatomic potential with an explicit water environment. Concerning the issue of determining the real manner of atomic dissolution for Pt NPs, numerous mathematical and first principles models have been developed and presented throughout the literature. Even recently another reactive potential model has been developed with a Grand-Canonical Monte Carlo (GCMC) method. However, the mechanism for dissolution in this method predicts the oxidation and then dissolution of a Pt_6O_8 species which is contradictory to some literature DFT calculations, and the MD simulations performed in this current work. It is also noted that the replication of oxidation of the NPs in this GCMC model have not been achieved with newer versions of codes.⁵³ It is believed that from this current work that the Pt_6O_8 species is a not experimentally favorable especially since with newer versions of the code the NPs reach an energy minimum without fully oxidizing. Dissolution rates and timings of atomic Pt are shown to be quite consistent across the 240 simulations carried out in the present investigation. Implementation of the restart commands in LAMMPS have also proven successful in recreating and reproducing these models.

The results of DFT calculations have shown that the dissolution of Pt from the (100) facet has the lowest dissolution energy, in agreement with the predictions of these MD simulations. The simulations further predict that the dissolution of Pt NPs are more favorable at O^* ML coverages below 0.5, which corresponds to the trend that adsorbed oxygen lowers the surface energies of the Pt NPs. This correlates well to previous work, in which the surface reconstruction of the oxidized Pt NPs increased from the initial NP structure as the O^* ML coverage increased, leading to the formation of a passive oxide film on the NP surface. Although it is common practice to compare

the oxidation and the dissolution of Pt surfaces and Pt NPs to the O* ML coverages, this descriptor does not describe the complete picture of atomic dissolution. This is because at 600 K dissolution of the Pt NPs is predicted for all of the NPs for at least one of the O* ML coverages while other NPs had all five coverages predict dissolution, with only the 0.25 O* ML having predicted dissolution at all of the NP sizes. Which illustrates that the size and morphology of the NPs is not a dominant factor in the dissolution of the Pt NPs compared to the adsorbates. This is also shown with the different NP morphologies and O* ML coverages that predicted dissolution at 450 K and did not predict dissolution at 600 K at discussed earlier. Therefore, the ratio of O* to the number of initial surface atoms is used to examine and compare the dissolution of the NPs in this study, and it is predicted that Pt dissolution is favorable below 40%. Although it is not determined what is the mechanism that caused dissolution at the lower temperatures compared to the higher temperatures the predictions of dissolution in the MD simulations are still reproducible.

With this the ECSA of the NPs are considered, however the results indicate that the kinetic interactions of the adsorbates and ion concentrations at the electrolyte interface play a considerably more significant role in the dissolution of Pt NPs, relative to the ECSA of the NPs.⁵⁴ Our research demonstrates that, in comparison to thermodynamic water models specifically produced by DFT and cluster expansion, a dynamic description of the water films produced on the NPs has a profound effect on the electrode-electrolyte interfaces which has been in agreement with experiments and Ab initio calculations.^{11,54,55}

The analysis of these simulations compared to literature shows that the binding of unique water structures, formed at oxidized electrode surfaces, defines the rate determining steps of dissolution of Pt atoms and the degradation of the Pt NPs.^{6,49} It is observed that the water structures have the same type of bonding that occurs with H⁺ ions in Zundel and Hydronium water structures,

as illustrated in Figures 8. In this work we must assure that the formation of these cations is possible and is done by comparing the formation energies and to the comparison of experimental literature.⁶ The heats of formation for these molecules are within reasonable calculations and it has been experimentally observed that the Pt (111) surfaces favor the Zundel cations to other cations and that the cation ratios to water are stable from 0 to 0.2, whereas for other noble metals such as Au the cations ratios are only stable at low values or intermediate values around 0.13.⁶ From these works the unique molecules and structures observed in the simulations are considered valid and shown in Figure 9.⁵⁶ It is also noted that H^+ ions produced in the simulations do not bond to O^* atoms to form H_2O , but instead remain at a distance of approximately 1.47 Å from the O^* atom.

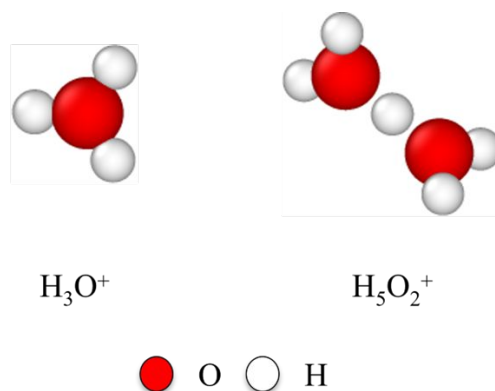


Figure 8- The Hydronium (H_3O^+) and Zundel ($H_5O_2^+$) cations.

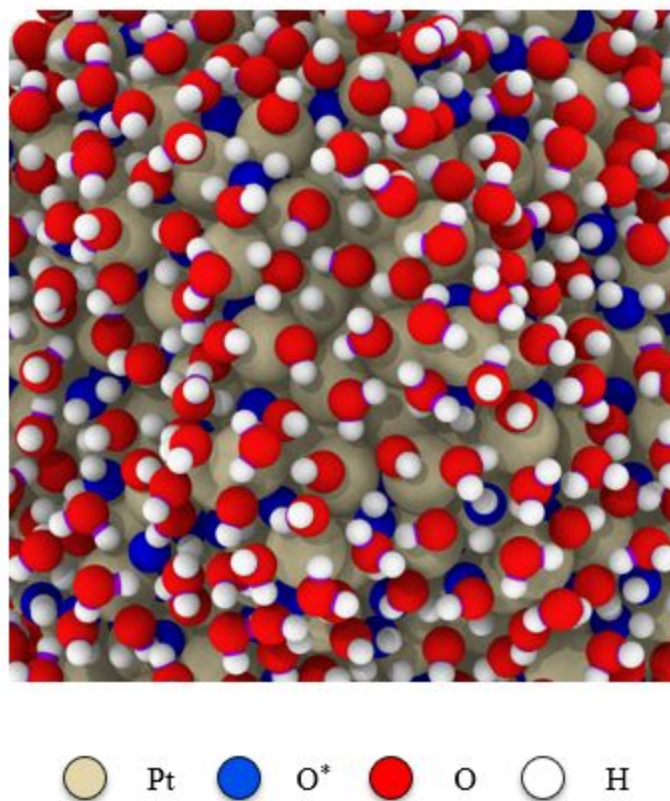


Figure 9- The dissociation of water molecules and the formation of unique water structure on the surface of the Pt NPs in the explicit water MD simulations.

The results indicate that the dynamics surrounding newly dissociated H^+ ions are possible driving factors for the movement of these ions between oxygen atoms, where H^+ ions near the nanoparticle surfaces are predicted to be pinned between oxygen atoms at equidistant locations in any of the simulations where the dissociation of water molecules occurs. This is because the implementation of the equation used in the QEq scheme (Equation 5) exhibits asymptotic charge transfer due to the absence of a distance-dependent charge transfer term implemented into COMB3 and QEq. Therefore, with this implementation there is an artifact in the potential which allows for charge transfer to occur over an infinite separation distance between atoms. It is believed that when atoms are close and within the 11.1 angstrom cutoff distance of the COMB3 potential that the

dissociation of water molecules and ion transport is predicted to occur at slower rates than in experiments. The following is the solution to Equation 5

$$E(P) = \sum_{ij}^n (\chi_i^0 q_i) + \frac{1}{2} \sum_{ij} q_i P_{ij} J_{ij} \quad , \quad \text{Eq. 5}$$

where P is an antisymmetric matrix, χ is the electronegativity of an atom, and q is the charge on an atom.⁴⁰

Conclusions

The durability and performance of fuel cells has been associated with the dissolution of the Pt NPs incorporated into the system. Although dissolution is known to be the leading degradation mechanism in fuel cells, the simulations presented in this work show that dissolution of the Pt NPs occurs more frequently with elevated operating temperatures. It is also determined the effect of the adsorbed species on the Pt NPs are more determinate in the selection of a rate determining step for Pt atom dissolution. However, no evident trend to predict the dissolution of the NPs, based on the either the size of the NPs or the O* ML coverages has been decerned, since dissolution is predicted at all of the simulated NP sizes and what is considered a random dissolution at the different ML coverages. However, it is also determined that dissolution is more dependent on the number of oxygen adsorbates as a percentage of the number of initial NP surface atoms is a more accurate descriptor, in showing that at lower percentages (less than 40%) less subsurface oxidation has occurred and a smaller platinum oxide film forms on the surface of the NP making it is easier for Pt atoms to dissolve.

With the development of this newly reproducible kinetic model in an explicit water environment, the scientific community will be able to better comprehend the degradation and dissolution of Pt NPs by further studying the interactions of adsorbates and the concentration of ions at the electrode-electrolyte interfaces. This work suggests that the bonding of unique water

structures is the determining factor for the degeneration and the dissolution of the Pt NPs. Future work in this area should focus on the use of explicit environment simulations to determine the effects of ions, their concentrations, and specific adsorption energies to further the fundamental understanding of the limiting kinetic reactions at the electrode-electrolyte interface, which will aid in the development of more efficient Pt fuel cells.

Acknowledgements

The authors acknowledge financial support from the US Department of Energy, Office of Science, Basic Energy Sciences, CPIMS Program, under Award No. DE-SC0018646. The authors also acknowledge that computational resources needed to perform classical molecular dynamics simulations for this research were provided by the Department of Defense High Performance Computing Modernization Program (DoD-HPCMP). We thank Douglas E. Wolfe for many helpful discussions.

References

- 1 Y. Kang, P. Yang, N. M. Markovic and V. R. Stamenkovic, *Nano Today*, 2016, **11**, 587–600.
- 2 K. A. Fichthorn and T. Yan, *J. Phys. Chem. C*, 2021, **125**, 3668–3679.
- 3 S. Campisi, M. Schiavoni, C. E. Chan-Thaw and A. Villa, *Catalysts*, 2016, **6**, 1–21.
- 4 M. J. Eslamibidgoli, J. Huang, T. Kadyk, A. Malek and M. Eikerling, *Nano Energy*, 2016, **29**, 334–361.
- 5 I. E. L. Stephens, J. Rossmeisl and I. Chorkendorff, *Science (80-.)*, 2016, **354**, 1378–1379.
- 6 Y. Tian, J. Hong, D. Cao, S. You, Y. Song, B. Cheng, Z. Wang, D. Guan, X. Liu, Z. Zhao, X. Z. Li, L. M. Xu, J. Guo, J. Chen, E. G. Wang and Y. Jiang, *Science (80-.)*, 2022, **377**, 315–319.
- 7 K. A. Fichthorn and T. Yan, *J. Phys. Chem. C*, 2021, **125**, 3668–3679.
- 8 B. M. Stühmeier, M. R. Pietsch, J. N. Schwämmlein and H. A. Gasteiger, *J. Electrochem. Soc.*, 2021, **168**, 064516.
- 9 J. Aarons, L. Jones, A. Varambhia, K. E. MacArthur, D. Ozkaya, M. Sarwar, C. K. Skylaris and P. D. Nellist, *Nano Lett.*, 2017, **17**, 4003–4012.

- 10 S. R. Dhanushkodi, S. Kundu, M. W. Fowler and M. D. Pritzker, *J. Power Sources*, 2014, **245**, 1035–1045.
- 11 Z. Duan and G. Henkelman, , DOI:10.1021/acscatal.1c02366.
- 12 M. Nesselberger, S. Ashton, J. C. Meier, I. Katsounaros, K. J. J. Mayrhofer and M. Arenz, 2011, 17428–17433.
- 13 A. R. Akbashev, *Curr. Opin. Electrochem.*, 2022, **35**, 101095.
- 14 A. S. Nair and B. Pathak, *Wiley Interdiscip. Rev. Comput. Mol. Sci.*, 2021, **11**, 1–19.
- 15 N. Goga, L. Mayrhofer, I. Tranca, S. Nedeia, K. Heijmans, V. Ponnuchamy and A. Vasileanu, *Catalysts*, 2021, **11**, 1–25.
- 16 V. M. Fernandez-Alvarez and M. H. Eikerling, *ACS Appl. Mater. Interfaces*, 2019, **11**, 43774–43780.
- 17 N. Bonnet and N. Marzari, *Phys. Rev. Lett.*, 2013, **110**, 1–5.
- 18 D. C. Ford, Y. Xu and M. Mavrikakis, 2005, **587**, 159–174.
- 19 Z. Gu and P. B. Balbuena, *J. Phys. Chem. C*, 2007, **111**, 9877–9883.
- 20 W. Schmickler, *J. Solid State Electrochem.*, 2020, 10–11.
- 21 E. Santos, P. Quaino and W. Schmickler, *Phys. Chem. Chem. Phys.*, 2012, **14**, 11224–11233.
- 22 J. Xie, X. Zhou, D. Luan and H. Jiang, , DOI:10.1021/acs.jctc.2c00017.
- 23 J. M. Sanchez, 1984, 334–350.
- 24 R. Drautz, 2019, **014104**, 1–15.
- 25 Y. Lysogorskiy, C. Van Der Oord, A. Bochkarev, S. Menon, M. Rinaldi, T. Hammerschmidt and R. Drautz, *npj Comput. Mater.*, 1–12.
- 26 M. Deng, F. Tushar, L. Bravo, A. Ghoshal, G. Karniadakis and Z. Li, 2021, 1–19.

- 27 A. Mahata, K. S. Rawat, I. Choudhuri and B. Pathak, *Catal. Sci. Technol.*, 2016, **6**, 7913–7923.
- 28 S. W. Rick, S. J. Stuart and B. J. Berne, *Dynamical fluctuating charge force fields: Application to liquid water*, .
- 29 A. K. Rappé and W. A. Goddard, *J. Phys. Chem.*, 1991, **95**, 3358–3363.
- 30 T. Liang, A. C. Antony, S. A. Akhade, M. J. Janik and S. B. Sinnott, *J. Phys. Chem. A*, 2018, **122**, 631–638.
- 31 R. Slapikas, I. Dabo and S. B. Sinnott, *J. Chem. Phys.*, 2020, **152**, 224702.
- 32 R. Slapikas, I. Dabo and S. B. Sinnott, *Comput. Mater. Sci.*, 2022, **209**, 111364.
- 33 I. T. McCrum, M. A. Hickner and M. J. Janik, *Langmuir*, 2017, **33**, 7043–7052.
- 34 M. J. Ungerer, D. Santos-Carballal, A. Cadi-Essadek, C. G. C. E. Van Sittert and N. H. De Leeuw, *J. Phys. Chem. C*, , DOI:10.1021/acs.jpcc.9b06136.
- 35 J. L. C. Fajín, M. N. D. S. Cordeiro and J. R. B. Gomes, *J. Phys. Chem. A*, 2014, **118**, 5832–5840.
- 36 Y. Wang and P. B. Balbuena, *J. Phys. Chem. B*, 2005, **109**, 14896–14907.
- 37 A. Michaelides and P. Hu, *J. Am. Chem. Soc.*, 2001, **123**, 4235–4242.
- 38 A. C. Antony, T. Liang and S. B. Sinnott, , DOI:10.1021/acs.langmuir.8b02315.
- 39 A. C. Antony, S. A. Akhade, Z. Lu, T. Liang, M. J. Janik, S. R. Phillpot and S. B. Sinnott, *J. Phys. Condens. Matter*, , DOI:10.1088/1361-648X/aa6d43.
- 40 T. Liang, T. R. Shan, Y. T. Cheng, B. D. Devine, M. Noordhoek, Y. Li, Z. Lu, S. R. Phillpot and S. B. Sinnott, *Mater. Sci. Eng. R Reports*, 2013, **74**, 255–279.
- 41 J. M. Hawkins, J. F. Weaver and A. Asthagiri, *Phys. Rev. B - Condens. Matter Mater. Phys.*, 2009, **79**, 125434.

- 42 D. Y. Chung, Y. H. Chung, N. Jung, K. H. Choi and Y. E. Sung, *Phys. Chem. Chem. Phys.*, 2013, **15**, 13658–13663.
- 43 T. Altantzis, I. Lobato, A. De Backer, A. Béch e, Y. Zhang, S. Basak, M. Porcu, Q. Xu, A. S anchez-Iglesias, L. M. Liz-Marz an, G. Van Tendeloo, S. Van Aert and S. Bals, *Nano Lett.*, 2019, **19**, 477–481.
- 44 M. J. Eckl, Y. Mattausch, C. K. Jung, S. Kirsch, L. Schmidt, G. Huebner, J. E. Mueller, L. A. Kibler and T. Jacob, *Electrochem. Sci. Adv.*, 2022, **2**, 1–13.
- 45 M. Alsabet, M. Grden and G. Jerkiewicz, *J. Electroanal. Chem.*, 2006, **589**, 120–127.
- 46 S. Arisetty, Y. Liu, W. Gu and M. Mathias, *ECS Meet. Abstr.*, 2015, **MA2015-02**, 1367–1367.
- 47 A. Allouche, *J. Comput. Chem.*, 2012, **32**, 174–182.
- 48 R. J. Zamora, B. P. Uberuaga, D. Perez and A. F. Voter, *Annu. Rev. Chem. Biomol. Eng.*, 2016, **7**, 87–110.
- 49 J. H. Bae, R. F. Brocenschi, K. Kisslinger, H. L. Xin and M. V. Mirkin, *Anal. Chem.*, 2017, **89**, 12618–12621.
- 50 B. D UNWEG and W. PAUL, *Int. J. Mod. Phys. C*, 1991, **02**, 817–827.
- 51 N. Gr onbech-Jensen, *Mol. Phys.*, 2020, **118**, 1662506.
- 52 T. Schneider and E. Stoll, *Phys. Rev. B*, 1978, **17**, 1302–1322.
- 53 B. Kirchhoff, C. Jung, H. J onsson, D. Fantauzzi and T. Jacob, *J. Phys. Chem. C*, 2022, **126**, 6773–6781.
- 54 Y. Tian, J. Hong, D. Cao, S. You, Y. Song, B. Cheng, Z. Wang, D. Guan, X. Liu, Z. Zhao, X. Li, L. Xu, J. Guo, J. Chen, E. Wang and Y. Jiang, 2022, **319**, 315–319.
- 55 S. Henrik and H. Kristoff, , DOI:10.1039/c8sc02495b.

- 56 H. H. Kristoffersen, T. Vegge and H. A. Hansen, *Chem. Sci.*, 2018, **9**, 6912–6921.